ADVANCED FUNCTIONAL MATERIALS

Supporting Information

for *Adv. Funct. Mater.*, DOI: 10.1002/adfm.202008088

Domain-Size-Dependent Residual Stress Governs the Phase-Transition and Photoluminescence Behavior of Methylammonium Lead Iodide

Kwang Jae Lee, Bekir Turedi, Andrea Giugni, Muhammad Naufal Lintangpradipto, Ayan A. Zhumekenov, Abdullah Y. Alsalloum, Jung-Hong Min, Ibrahim Dursun, Rounak Naphade, Somak Mitra, Iman S. Roqan, Boon S. Ooi, Omar F. Mohammed, Enzo Di Fabrizio, Namchul Cho, and Osman M. Bakr**

Submitted to ADVANCED FUNCTIONAL MATERIALS

Supporting Information

Domain-size-dependent residual stress governs the phase-transition and photoluminescence behavior of methylammonium lead iodide

Kwang Jae Lee[#], Bekir Turedi[#], Andrea Giugni[#], Muhammad Naufal Lintangpradipto, Ayan A. Zhumekenov, Abdullah Y. Alsalloum, Jung-Hong Min, Ibrahim Dursun, Rounak Naphade, Somak Mitra, Iman S. Roqan, Boon S. Ooi, Omar F. Mohammed, Enzo Di Fabrizio, Namchul Cho[*] and Osman M. Bakr[*]

Dr. K. J. Lee, B. Turedi, Dr. A. Giugni, M. N. Lintangpradipto, A. A. Zhumekenov, A. Y. Alsalloum, Dr. I. Dursun, Dr. R. Naphade, Prof. O. F. Mohammed, Prof. E. D. Fabrizio, Prof. O. M. Bakr
Physical Science and Engineering (PSE) Division
King Abdullah University of Science and Technology (KAUST), Thuwal 23955-6900, Kingdom of Saudi Arabia
[*]Email: osman.bakr@kaust.edu.sa

Dr. K. J. Lee, B. Turedi, A. A. Zhumekenov, A. Y. Alsalloum, Dr. I. Dursun, Dr. R. Naphade, Prof. O. M. Bakr
KAUST Catalysis Center (KCC)
King Abdullah University of Science and Technology (KAUST), Thuwal 23955-6900, Kingdom of Saudi Arabia

Dr. J.-H. Min, Dr. S. Mitra, Prof. I. S. Roqan, Prof. B. S. Ooi,
Division of Computer, Electrical and Mathematical Sciences and Engineering
King Abdullah University of Science and Technology (KAUST), Thuwal 23955-6900, Kingdom of Saudi Arabia

Dr. J.-H. Min, Prof. B. S. Ooi
Photonics Laboratory
King Abdullah University of Science and Technology (KAUST), Thuwal 23955-6900, Kingdom of Saudi Arabia

Prof. E. D. Fabrizio
Department of Applied Science and Technology
Politecnico di Torino, Torino 10129,
Italy

Prof. N. C. Cho
Department of energy systems engineering, Soonchunhyang University, Asan 31538, South Korea

[*]Email: chon7@sch.ac.kr

[#]Contributed equally to the work

Keywords

Perovskite, $MAPbI_3$, residual stress, domain size, photoluminescence

We report in **Figure S1** all the XRD patterns collected for single-crystalline (SC), polycrystalline (PC), highly oriented crystalline (HOC), and ground powder of SC (GSC) $MAPbI_3$ perovskites aside with acquisition temperature. We plot the spectra collected at 300 K after grinding each sample with red lines to evidence the same origin and composition of the $MAPbI_3$ crystals.

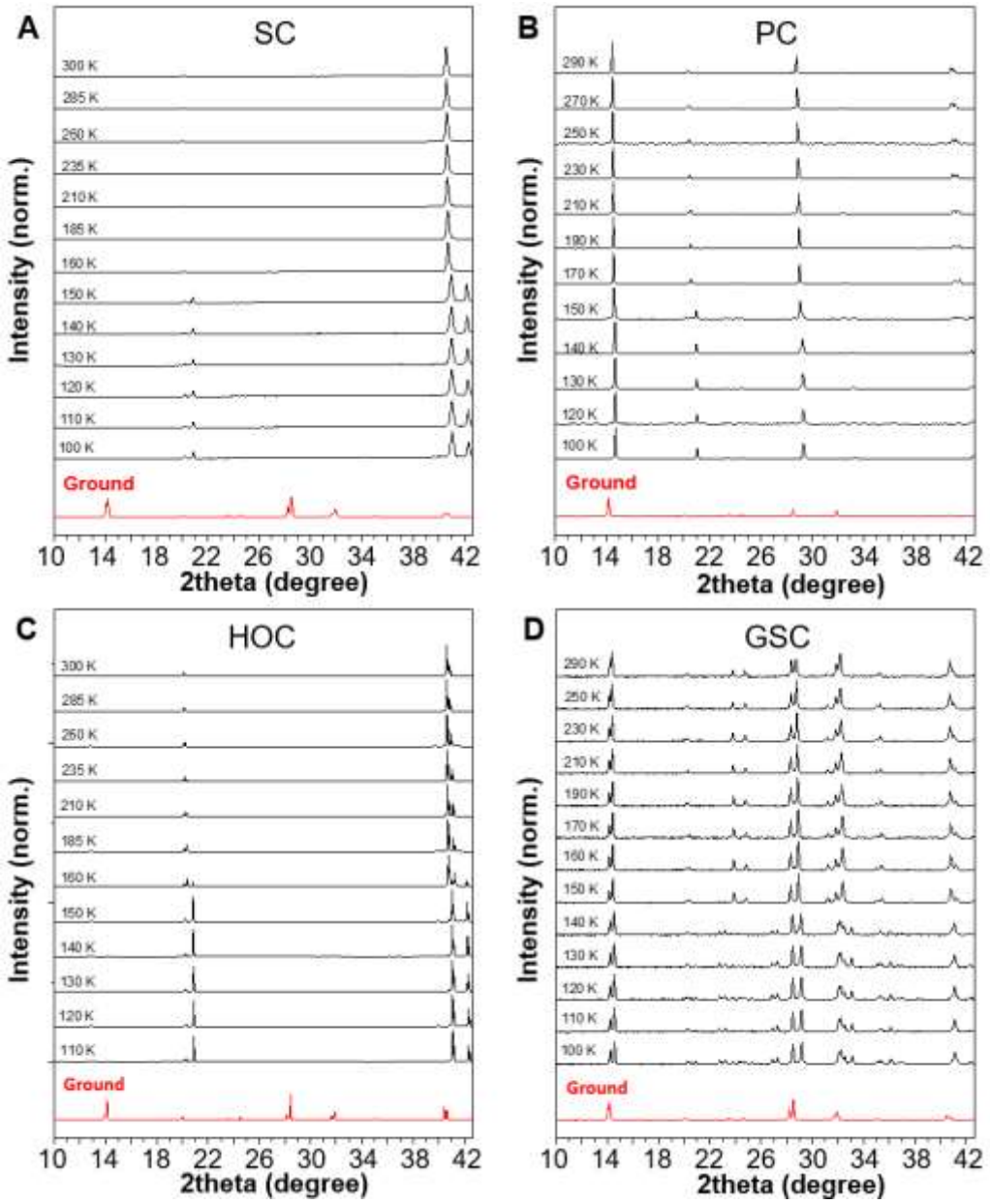

Figure S1. Temperature-dependent XRD of A) single-crystalline (SC), B) polycrystalline (PC), C) highly oriented crystalline (HOC) $MAPbI_3$ perovskites, and D) ground powder of SC $MAPbI_3$ perovskite (GSC).

Figure S2 shows representative sets of XRD diffraction spectra, where we labeled the main peaks with the corresponding plane's index. The SC sample undergoes a sharp and homogeneous phase transition between 150 and 160 K, while HOC, PC, and GSC perovskites experience an inhomogeneous phase transition extending tens of degrees, from a tetragonal to an orthorhombic prevalence while rising the temperature.

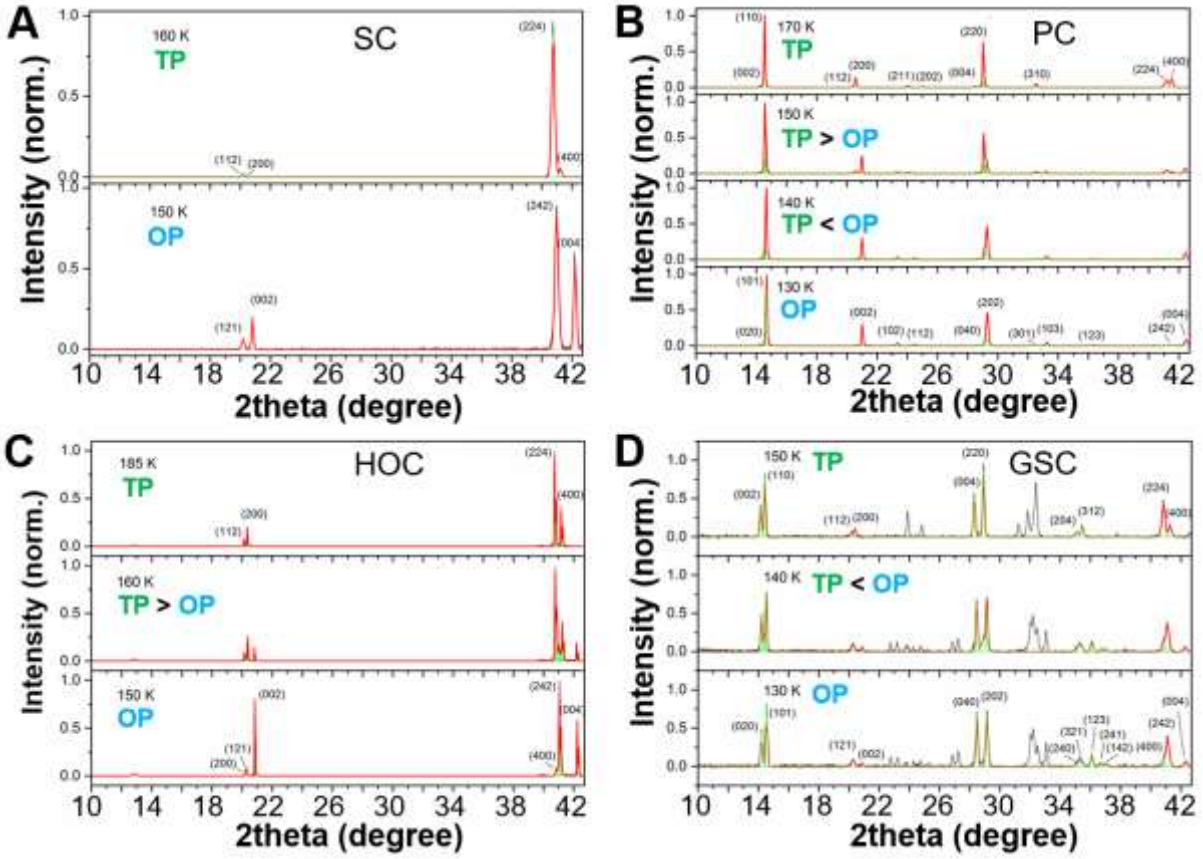

Figure S2. Representative temperature-dependent XRD spectra for D) SC, B) PC, C) HOC and D) GSC $MAPbI_3$ perovskite samples before/after the phase transition. (TP: tetragonal phase and OP: orthorhombic phase)

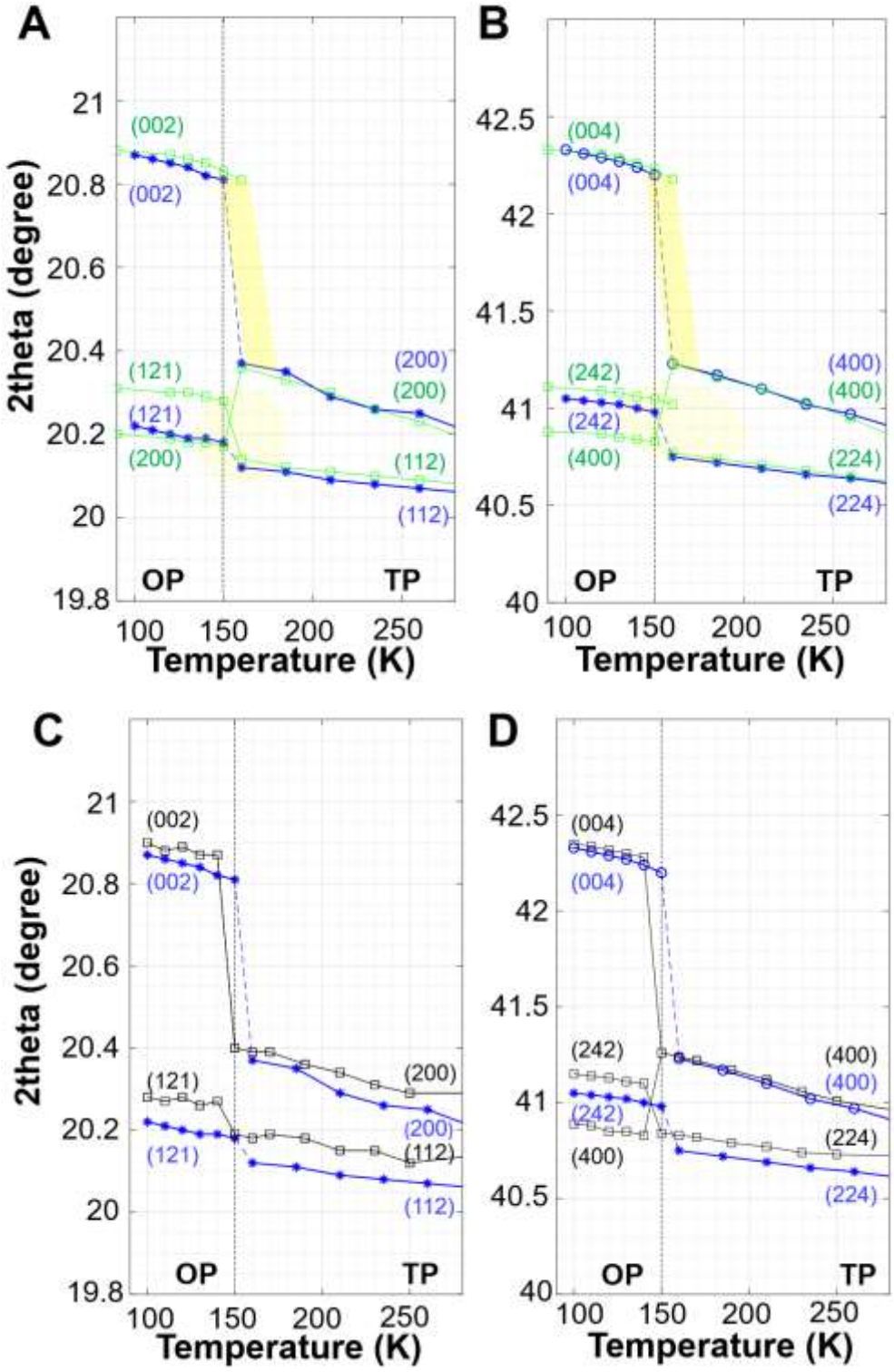

Figure S3. Temperature-dependent XRD 2theta peaks of SC (blue color), HOC (green color) and GSC (black color) $MAPbI_3$ perovskites by increasing the temperature from 80 K to 300 K in the range from 20° to 21° and 40.5° to 42.5°. A) and B) show the visualized XRD peak positions of SC and HOC samples for indicating planes, while C) and D) show the ones of SC and GSC $MAPbI_3$ perovskites for the same planes. The direct comparison evidences the similarities or differences between the three samples directly conducible to peculiar strain conditions.

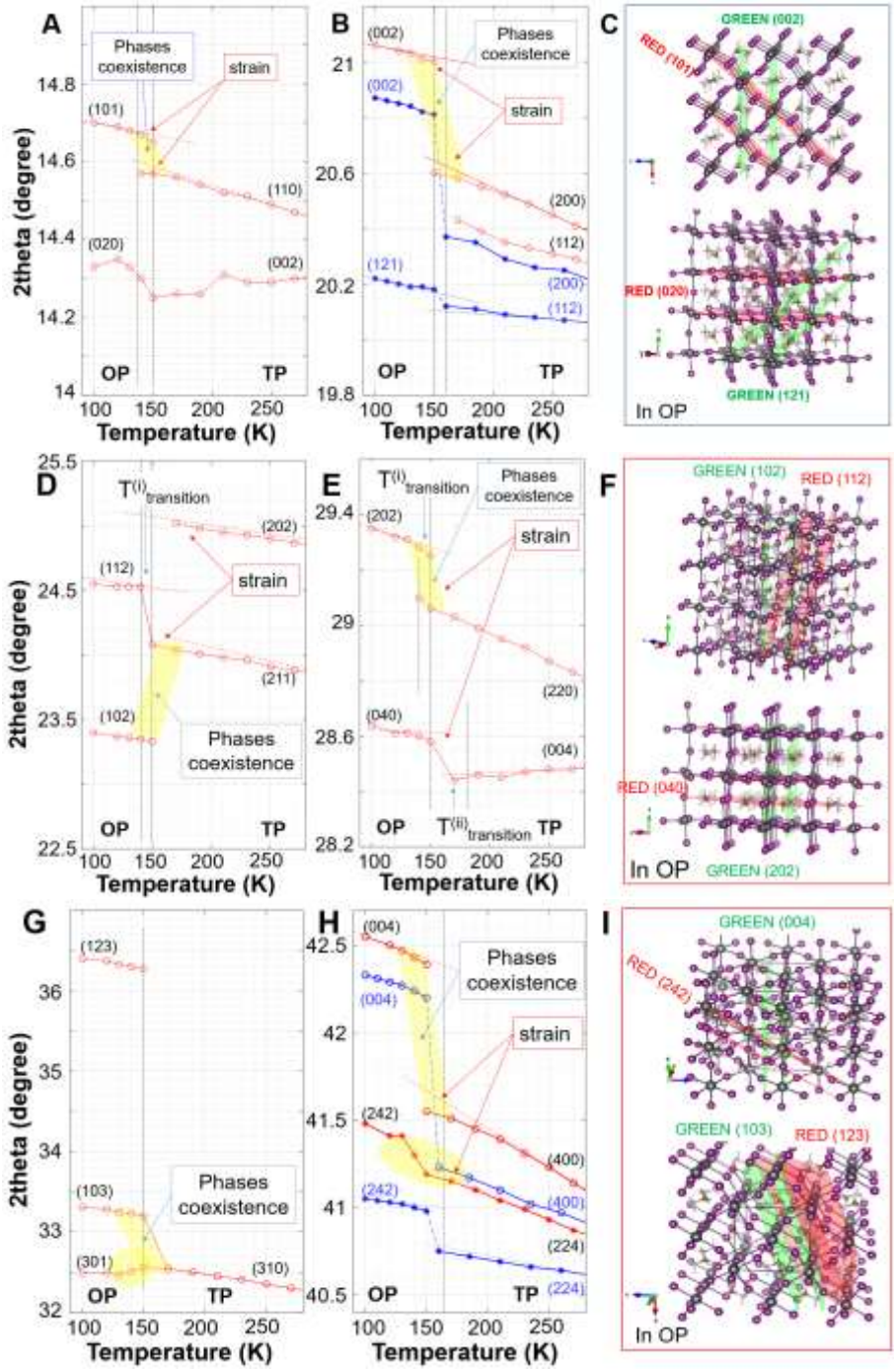

Figure S4. A), B), D), E), G) and H) Temperature-dependent XRD 2theta peaks of SC (blue color) and PC (red color) perovskites labeled with the corresponding crystallographic planes in OP and TP. The visual comparison evidences the similarities or differences between the two samples. The graphical illustration of crystallographic planes, in green and red colors, are shown on the calculated crystal structures for the orthorhombic phase in C) planes (002), (101), (020) and (121), F) planes (102), (112), (040), and (202), and I) planes (004), (242), (103), and (123).

We analyzed XRD spectra considering a K_α doublet as the exciting source of the scattered signal collected. For this reason, as shown in **Figure S5**, we use a model function composed of a Gaussian pair (black lines), with intensity ratio ½ and relative angular shift predetermined by a spectral calibration, convoluted by the instrumental resolution (red Gaussian profile). A χ^2 minimizations allowed to evaluate experimental meaningful parameters and uncertainties, as position and FWHM of each peak (blue dots). The Gaussian' FWHM, Γ, was obtained as ~2.355 σ. Representative analysis examples are reported in **Figure S5** corresponding to the planes (242) and (004) at about 41° and 42.3° for (**A**) (**B**) the as-prepared SC sample at, respectively, 100 K and 150 K superimposed by analytic model. The table reports the position center, sigma, and peaks area. **Figure S5** (**C**), (**D**), and (**E**) show XRD spectra of the PC sample collected for the three significant temperatures, 140, 150, 190 K, respectively in the orthorhombic, the phase transition, the tetragonal phases. **Figure S5** (**D**) indicates the coexistent of the two phases.

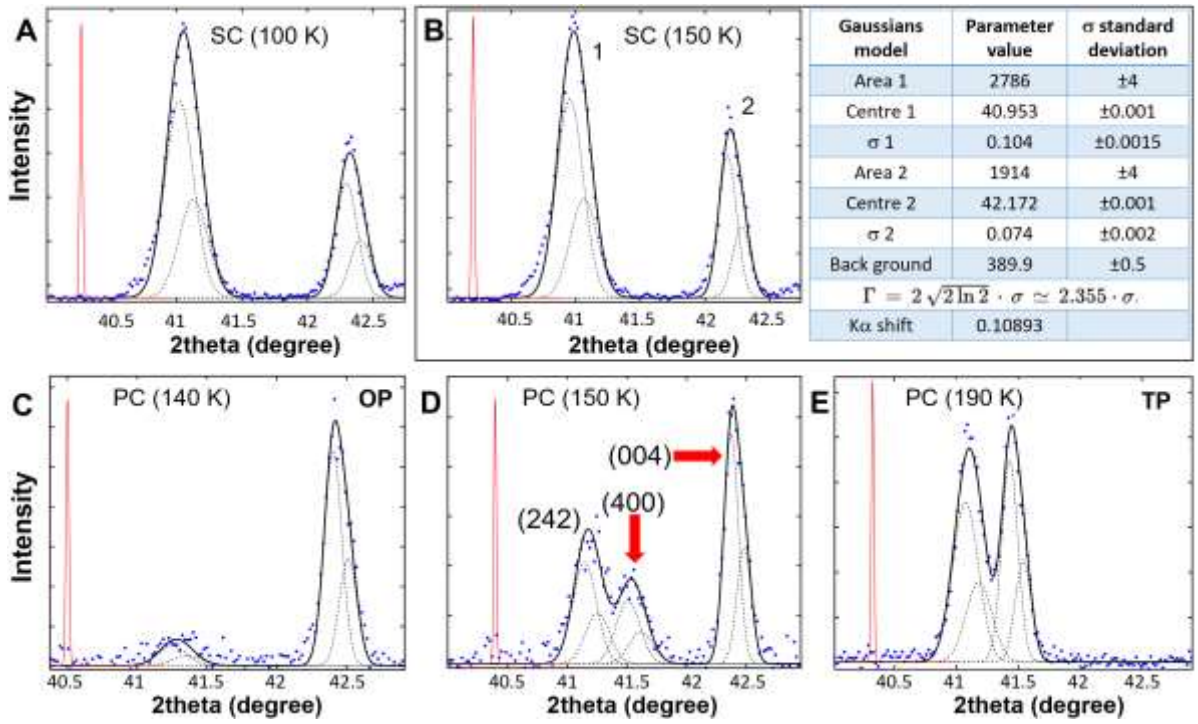

Gaussians model	Parameter value	σ standard deviation
Area 1	2786	±4
Centre 1	40.953	±0.001
σ 1	0.104	±0.0015
Area 2	1914	±4
Centre 2	42.172	±0.001
σ 2	0.074	±0.002
Back ground	389.9	±0.5
$\Gamma = 2\sqrt{2\ln 2}\cdot\sigma \simeq 2.355\cdot\sigma$		
Kα shift	0.10893	

Figure S5. Representative XRD spectra (blue dots) of the SC perovskite at A) 100 K and B) 150 K, and the PC perovskite at C) 140 K, D) 150 K, and E) 190 K, respectively that correspond to the (242) and (004) planes for the SC perovskite at about 41° and 42.3° and also to the (400) for the PC sample at about 41.6°. A Gaussian K_α doublet (dashed black line) convolved with the experimental resolution was used as a proper function to model each peak in the XRD reconstructed spectra (continuous black line). Sharp Gaussians, a continuous red line on the left of each graph, show the experimental resolution. The table shows parameters and uncertainties determined by the minimization routine for peaks 1 and 2 in the XRD spectrum of the SC perovskite shown in Figure S5B. The XRD

spectrum of the PC sample reported in panel D) evidences the coexistence of both phases indicated with red arrows.

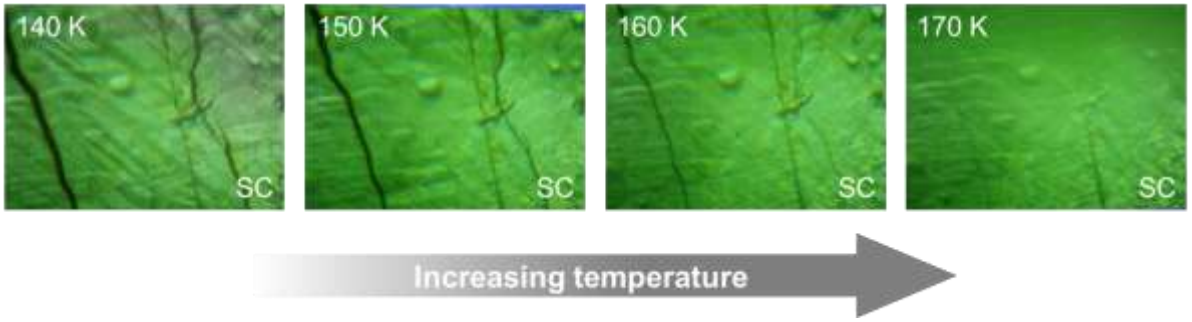

Figure S6. Optical microscope images of SC $MAPbI_3$ surface by increasing the temperature through the phase-transition region.

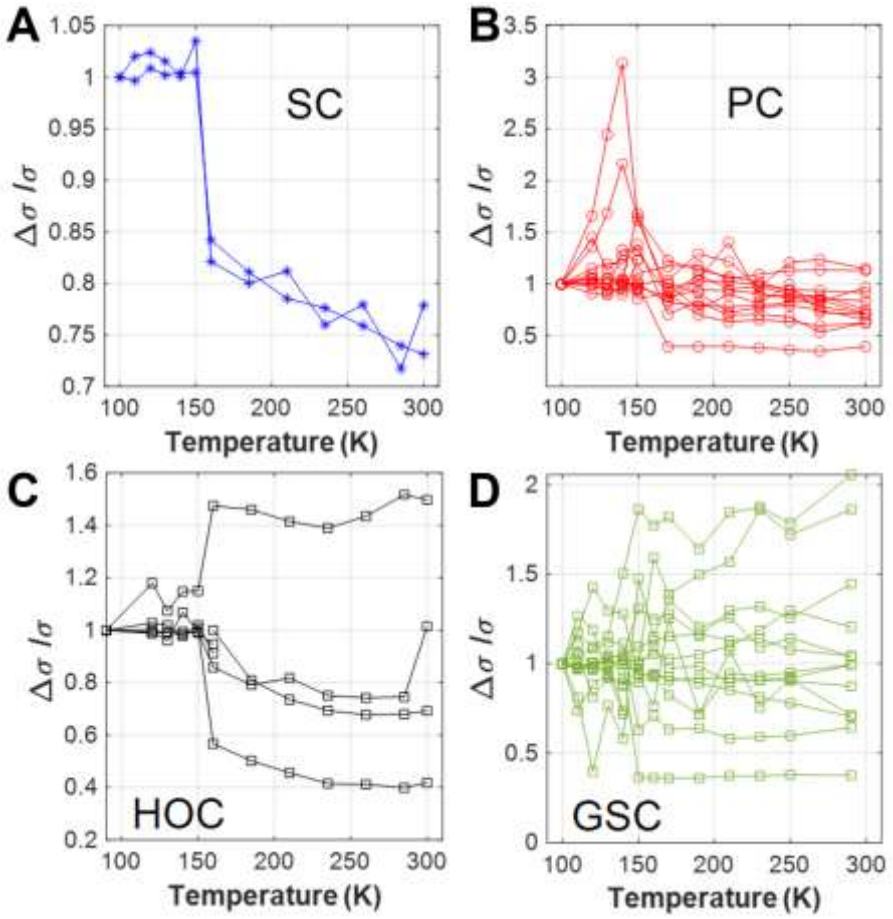

Figure S7. Temperature-dependent variation of the XRD peaks' FWHM, expressed as $\Delta\sigma/\sigma(100\ K) = (\sigma(T)-\sigma(100\ K))/\sigma(100\ K)$, for A) the SC perovskite (002) and (121) planes, B) the PC perovskite (020), (101), (002), (102), (112), (040), (202), (301), (103), (123), (242), (202), (400), and (004) planes, C) the HOC perovskite (200), (121), (002), (400), (242), and (004) planes, and D) the GSC sample (020), (101), (121), (002), (040), (202), (242), (321), (123), (241), (142), (400), (224), and (004) planes. Significantly different behaviors for the

three crystal types indicate heavily different inhomogeneous strain and stress conditions. σ is the Gaussian standard deviation.

We measured the Raman vibrational spectra of PC and SC $MAPbI_3$ perovskites to investigate the lattice rearrangements before and after the phase-transition (**Figure S8A and S8B)**. The PC sample for surface-enhanced Raman scattering (SERS) was prepared by drop-casting on 50 nm-thick Au layer on a mica substrate. The Au nanostructured surface intensified the Raman signal by the plasmonic enhancement effect.

Figure S8C and **S8D** show the optical microscope images of the surface area of PC and SC samples, respectively. The insets show the sample surface illuminated by the laser radiation after the optical Bragg gratings filter. The notch filter rejects the elastic line scattering (black cross in insets of Figure **S8C** and **S8D**), letting pass the Raman and broadband fluorescence signals, easily visible on the samples as a bright spot.

The experimental condition used to perform Raman scattering has been described in the Experimental Section in the main text. To confirm the crystal quality of our samples, we checked for the presence of the PbI_2 spectral signature, which is known to appear as a consequence of laser-induced photodegradation of the perovskite's structures. It was not present in our spectra.

We note that the principal limit to the Raman signal detectability has been the parasitic luminescence emission excited in quasi resonance condition at 633 nm. Strong PL was by far the largest signal, and thus a severe source of statistical noise for the visibility of the Raman modes. In the case of the SC, each spectrum was obtained after the accumulation of long-lasting 10 × 300 s integration time, and the Raman contribution was afterward isolated subtracting a 6^{th} order polynomial used to model the PL. Differently, in the case of the PC perovskite, we got clear results subtracting a multi-shaped curve. **Figure S9A** and **Figure S11** show representative low frequency Stokes and anti-Stokes Raman spectra of SC and PC samples obtained. In agreement with the literature,[1] we identify the cage-signature in the peaks at the very low energies below 100 cm^{-1}. A low-middle energy band of closely packed Raman peaks (between 100 and 400 cm^{-1}) corresponds to the MA, being very sensitive to the cage conformation. The higher energy Raman-active modes have been exclusively assigned to the MA cation dynamics.

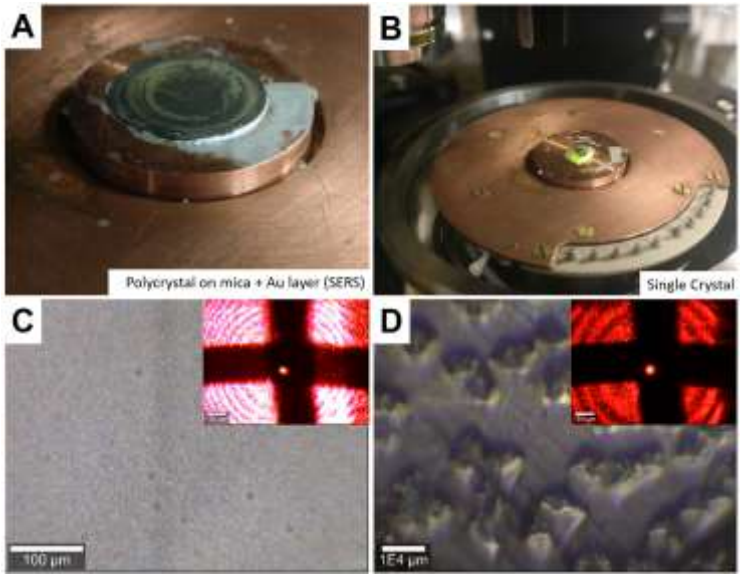

Figure S8. Investigated samples by Raman spectroscopy. Photographs of A) PC and B) SC samples glued on the cryostat cold finger. Optical microscope images of C) PC and D) SC samples (×100). Insets show the same optical microscope images obtained under laser illumination of the samples. The intense fluorescence spot at the center of the dark cross marks the volume scattering emission from the sample.

In **Figure S11** and **S12,** we report exemplary Lorentzian function decomposition of the main peaks in Raman spectra for SC and PC samples. Accurate determination of low-frequencies peaks, obtained from the corresponding Stokes and Anti-Stokes distances, allows modes identification and assignation in agreement with literature results on the normal modes decomposition.

A sharp change in spectral profile of the SC $MAPbI_3$ perovskite depicts a clear phase-transition at the temperature of 155 K (**Figure S9B)**. The octahedra twist (TO) modes and the Nodding donkey around the N in the MA cation disappear at the higher temperature. **Figure S10A** illustrates a different result for the PC perovskite. General band broadening and the compresence of characteristic peaks of both phases in an extended range of temperatures indicate a smooth transition from the orthorhombic to the tetragonal phase. A similar smooth transition is also observed in the emission profiles reported in **Figure S10B** versus temperature. A refined picture can be obtained considering the Raman modes that most indicate the available space and degrees of freedom of the cation; in the spectrum of the PC sample, they are the two bands in the range 80 to 300 cm^{-1}. Their presence and frequency broadening indicate the effect of disorder in the MA torsional modes. Tracking the bands' shift as a function of temperature, we observed a gradual red-shift in the centers of mass and a gradual suppression of the high energy nodding donkey around N mode. The spectral changes,

progressively induced by increasing temperature, indicate an inhomogeneous change at the cage level, suggesting a volumetric space change different from what was observed for the SC cage. This dissimilarity, ascribable to a domain-size-dependent strain, confirms XRD results and supports the presence of qualitative different residual stresses between the two types of $MAPbI_3$ perovskites.

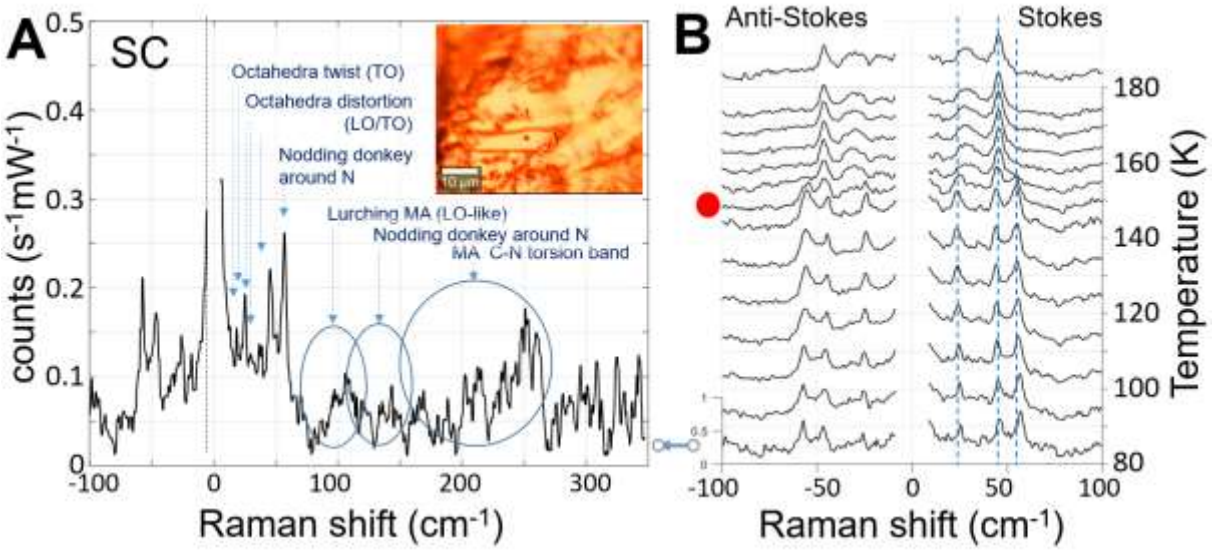

Figure S9. A) Raman spectrum of the SC $MAPbI_3$ perovskite at 80 K where are indicated main modes and bands. Inset shows the sample surface. B) Low-frequency Raman spectra in the temperature range from 80 to 180 K. Phase transition temperature was denoted as a red dot. Quasi-resonant absorption of the 633 nm excitation line determines the thermodynamic equilibrium of the phononic population in the material by the Stoke to anti-Stokes intensity ratio. The red dot shows the phase-transition between 155 K and 160 K.

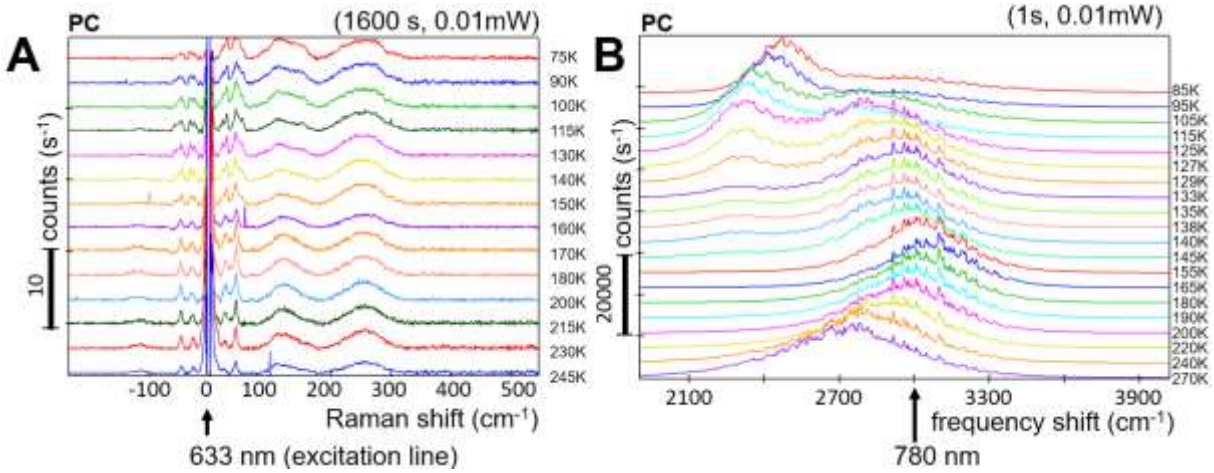

Figure S10. A) Low-frequency SERS spectra and B) photoluminescence of the PC sample acquired from the same scattering volume on the sample.

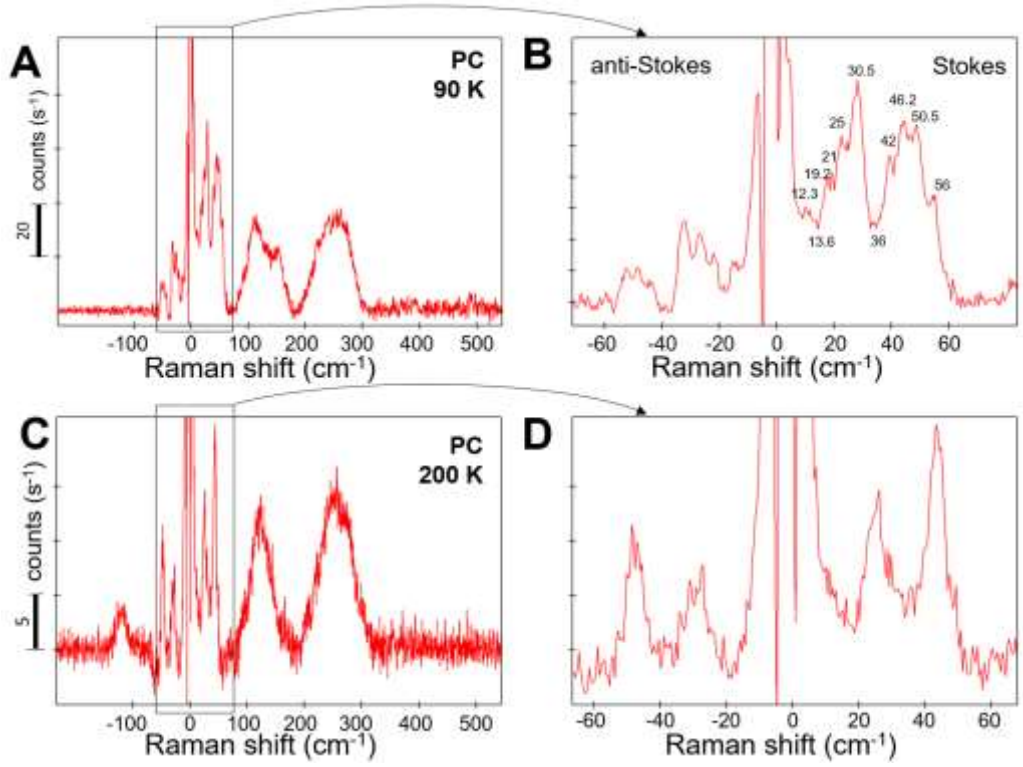

Figure S11. Low-frequency SERS signals (after PL and background removal) from the PC sample in A) orthorhombic and C) tetragonal phases. B) and D) are the corresponding spectral detail centered at zero, characterized by several peaks, in agreement with the theoretical calculation of literature.

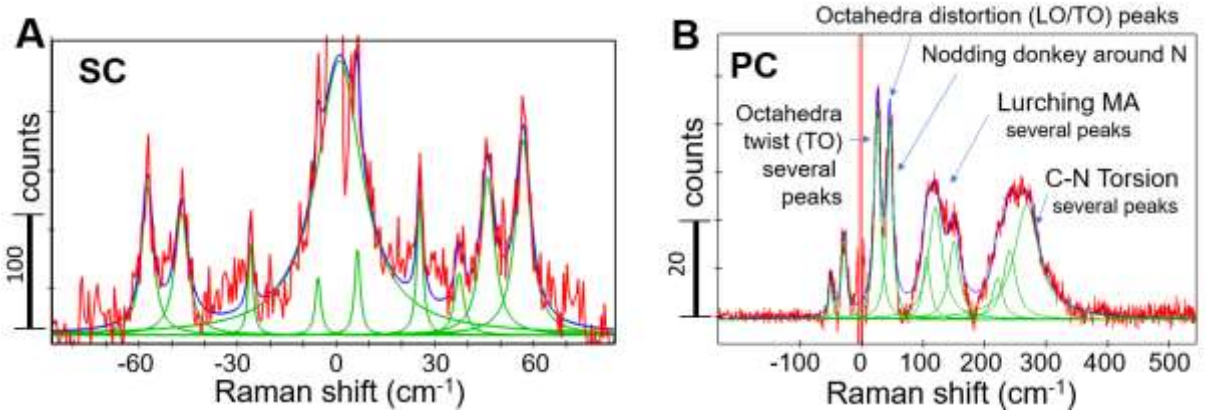

Figure S12. Lorentzian line shape analysis of the low-frequency Raman spectrum of (A) SC and (B) PC samples collected at about 80K. In the case of the PC sample, we report most of the identified peaks in **Figure S11B**.

Reference

[1] M. A. Pérez-Osorio, R. L. Milot, M. R. Filip, J. B. Patel, L. M. Herz, M. B. Johnston, F. Giustino, *J. Phys. Chem. C* **2015**, *119*, 25703.

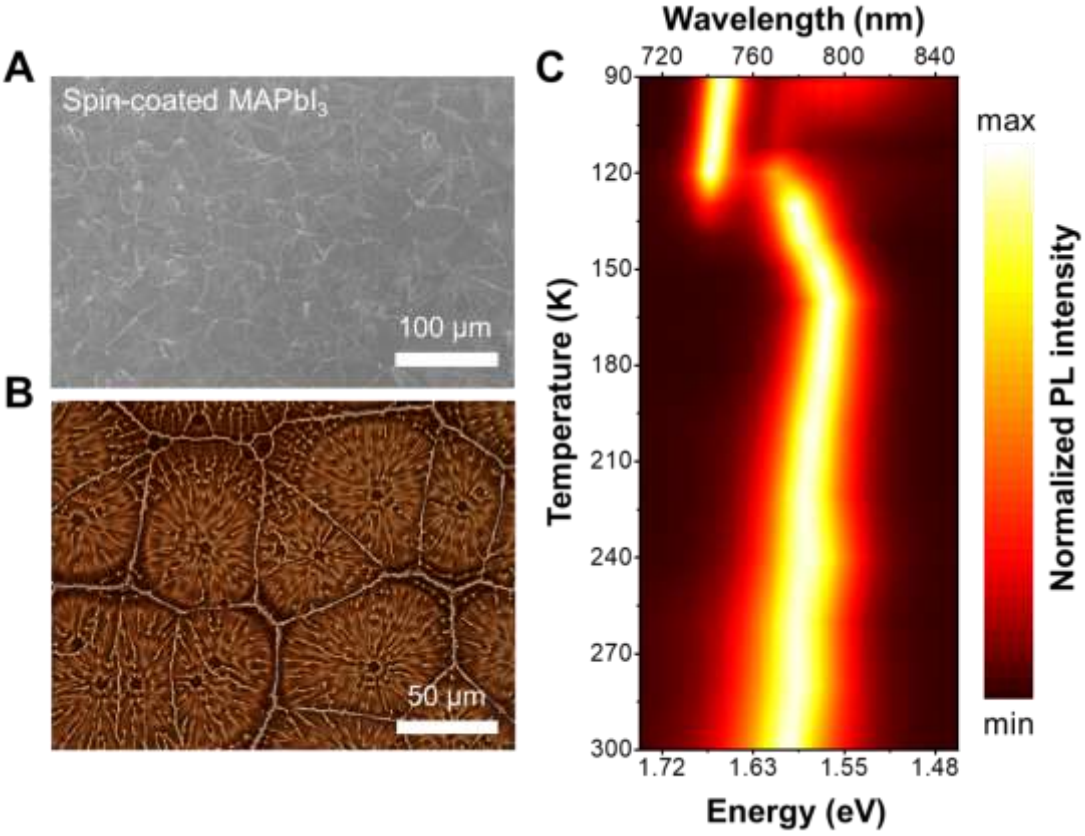

Figure S13. A) The SEM image, B) the optical microscope image in transmission mode, and C) the temperature-dependent photoluminescence (TDPL) pattern of the PC perovskite with an average domain size of 100 μm.

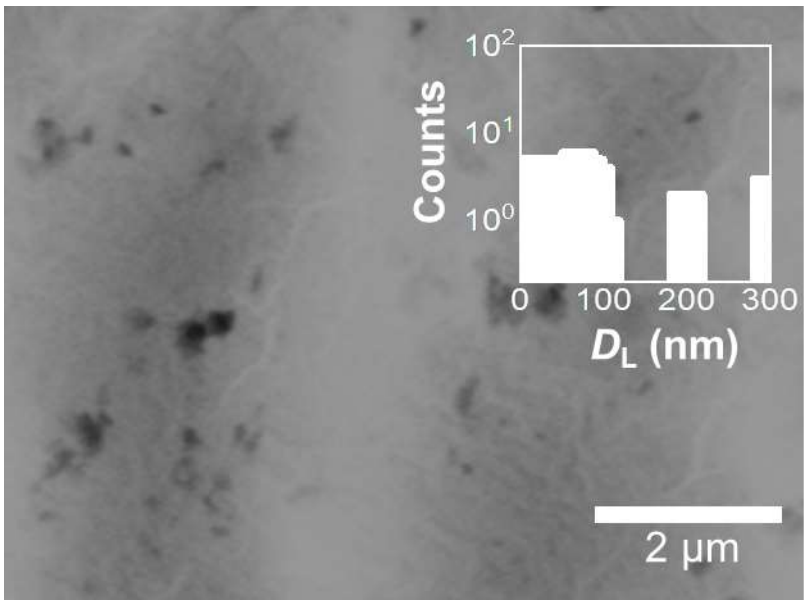

Figure S14. SEM images of ground $MAPbI_3$ perovskites

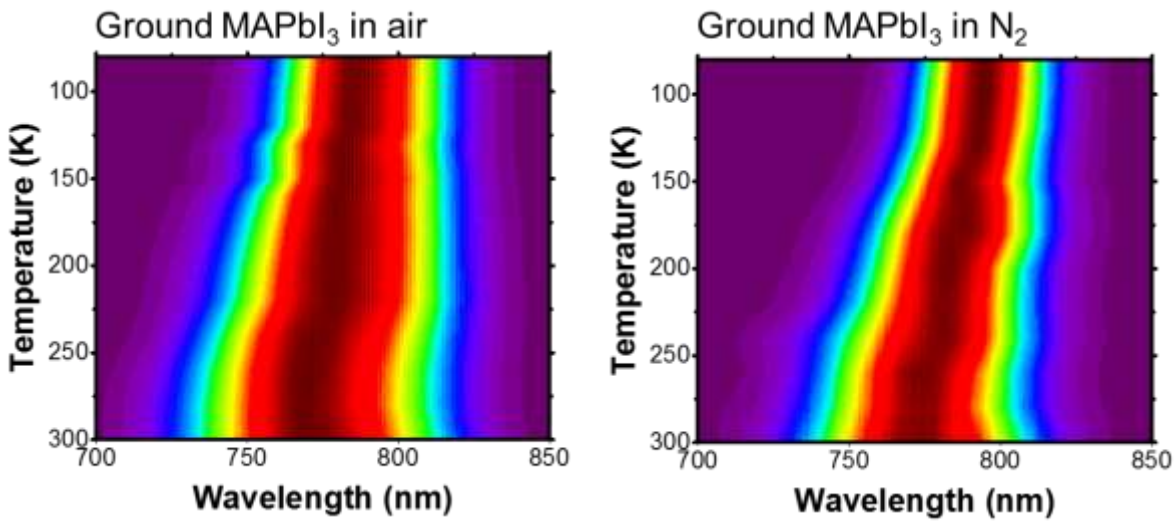

Figure S15. TDPL spectra of ground $MAPbI_3$ perovskites measured in air and nitrogen atmosphere.

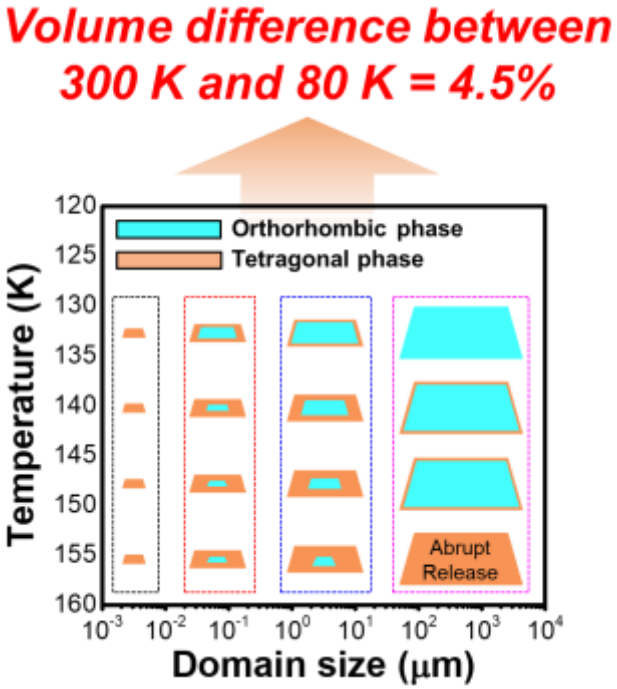

Figure S16. The phase-transition begins at the domain's surface and proceeds inwards to the domain's cross-section.

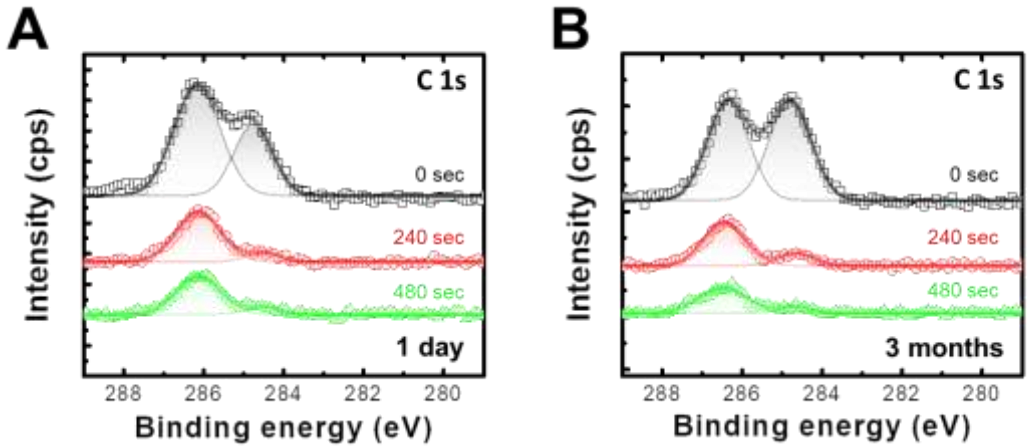

Figure S17. X-ray Photoelectron Spectroscopy (XPS) depth profiling of carbon rates for the SC perovskite after exposing in air for A) one day and B) 3 months.